PCCP

PAPER

View Article Online
View Journal | View Issue

Cite this: *Phys. Chem. Chem. Phys.*, 2016, **18**, 25080

Ultrafast electronic energy relaxation in a conjugated dendrimer leading to inter-branch energy redistribution†

D. Ondarse-Alvarez,[a] S. Kömürlü,[b] A. E. Roitberg,[b] G. Pierdominici-Sottile,[a] S. Tretiak,[c] S. Fernandez-Alberti*[a] and V. D. Kleiman*[b]

Received 24th June 2016,
Accepted 8th August 2016

DOI: 10.1039/c6cp04448d

www.rsc.org/pccp

Dendrimers are arrays of coupled chromophores, where the energy of each unit depends on its structure and conformation. The light harvesting and energy funneling properties are strongly dependent on their highly branched conjugated architecture. Herein, the photoexcitation and subsequent ultrafast electronic energy relaxation and redistribution of a first generation dendrimer (**1**) are analyzed combining theoretical and experimental studies. Dendrimer **1** consists of three linear phenylene-ethynylene (PE) units, or branches, attached in the *meta* position to a central group opening up the possibility of inter-branch energy transfer. Excited state dynamics are explored using both time-resolved spectroscopy and non-adiabatic excited state molecular dynamics simulations. Our results indicate a subpicosecond loss of anisotropy due to an initial excitation into several states with different spatial localizations, followed by exciton self-trapping on different units. This exciton hops between branches. The absence of an energy gradient leads to an ultrafast energy redistribution among isoenergetic chromophore units. At long times we observe similar probabilities for each branch to retain significant contributions of the transition density of the lowest electronic excited-state. The observed unpolarized emission is attributed to the contraction of the electronic wavefunction onto a single branch with frequent interbranch hops, and not to its delocalization over the whole dendrimer.

Introduction

A fundamental requirement in the attempt to mimic natural photosynthesis involves a comprehensive knowledge of synthetic light harvesting materials and the intramolecular mechanisms of the energy redistribution triggered after photoexcitation.[1–6] Light absorption involving multiple equivalent chromophore units introduces interplay and competition between relative time scales for intra- and inter-molecular chromophore energy transfers as well as electronic and vibrational transfer processes. These initial electronic/vibrational energy transfer mechanisms are responsible for the efficiency in the transformation of photon energy into other usable forms of energy.[7–10]

Advances in organic synthesis enable the development of new light-harvesting materials that can potentially improve the efficiency of organic photovoltaic cells in converting the energy of light directly into electricity. Among these novel materials, dendritic macromolecules have attracted special attention due to their well-defined regular structures with numerous individual chromophore units.[3,11–23] Dendrimers are highly branched conjugated macromolecules with complex, well-defined three dimensional structures.[24–26] The highly polarizable and spatially extended π-electron manifold is responsible for many of their unique electronic and photophysical properties that make them suitable for a broad range of technological applications. A recent improvement in the synthesis of dendrimers allows new designs introducing functional groups in order to explore alternatives in their architecture that can lead to new optoelectronic properties.

Since the original work by Moore and coworkers, the family of dendrimers comprised of phenylene ethynylene (PE) units has been the focus of several experimental and theoretical studies.[20,27–33] They exhibit both collection and energy transfer processes that are of interest in photosynthetic systems.[27–29] The large number of chromophore units in their structures increases the molar absorptivity. PE dendrimers have been shown to undergo highly efficient and unidirectional energy transfer associated with their efficient energy funneling.[31,33–42] The complex interplay between atomic motions, excited-state populations,

[a] *Departamento de Ciencia y Tecnologia, Universidad Nacional de Quilmes/CONICET, B1876BXD Bernal, Argentina. E-mail: sfalberti@gmail.com*
[b] *Department of Chemistry, University of Florida, Gainesville, Florida 32611, USA. E-mail: kleiman@chem.ufl.edu*
[c] *Theoretical Division, Center for Nonlinear Studies (CNLS), and Center for Integrated Nanotechnologies (CINT), Los Alamos National Laboratory, Los Alamos, NM 87545, USA*

† Electronic supplementary information (ESI) available. See DOI: 10.1039/c6cp04448d

and localization/delocalization of excitations has been a point of intense research for different building blocks of PE dendrimers. As a result, the coherent control of excited-state dynamics in PE dendritic macromolecules has been shown to be possible.[42] More recently, a consistent experimental-theoretical description of excited-state dynamics in an unsymmetrical PPE dendrimer has shown that its electronic intramolecular energy-transfer mechanism after light absorption involves the ultrafast collapse of the photoexcited wave function due to nonadiabatic electronic transitions.[43]

The complex electronic dynamics in PE dendrimers is determined by nonadiabatic dynamics involving multiple coupled electronic excited states. Following light-absorption, the multiple photoinduced pathways to energy relaxation and redistribution involve internal conversion processes and changes in the spatial localization of the electronic transition density. Previous works have measured the excited state populations as well as the energy transfer and vibrational relaxation processes using time-resolved emission and absorption techniques.[22,40,41,44] To complement this, simulation of these photophysical processes can be achieved using non-adiabatic excited state molecular dynamics (NA-ESMD).[35–37] This methodology has been successfully used to simulate the intramolecular flow of the excess energy in many large organic conjugated molecules including different PE dendrimers.[39] The role played by thermal structural fluctuations in the building blocks of PE dendrimers during the dynamics of relaxation of high-energy excited states has been revealed *via* analysis based on the evolution of transition density localization.[35,45]

The flexibility of the three dimensional architecture of PE dendrimers depends on the steric effects between chromophore units[31,46–48] and it can be modulated by the incorporation of bulky end-groups into their highly branched structures. The scope of their conformational landscape has a significant impact on the localization of the electronic transition densities and, therefore, effects on intra- and inter-unit energy transfer. The degree of conformational disorder strongly influences the available through-space and sequential through-bond energy transfer mechanisms.[37]

In this work, we present the results of a combined theoretical-experimental study elucidating ultrafast electronic energy relaxation and the redistribution of a first generation dendrimer (**1**)[49] (see Fig. 1). For this purpose, time-resolved spectroscopy and NA-ESMD simulations have been performed. Dendrimers with chromophores of the same conjugation length lead to compactness, resulting in a lack of energy gradient. This is the case for dendrimer **1**, which consists of three equivalent linear PE units attached in the *meta* position to a central group opening the possibility of inter-branch energy transfer. In the ground electronic-state, the *meta* branching breaks the conjugation giving rise to localized excitations.[47] The presence of transient electronic couplings and delocalization of excited-state wavefunctions have been previously supported by *ab initio* calculations and the experimental results.[39,41,45,50,51] The variation in time of the strength of such nonadiabatic couplings and the extent of exciton delocalization modulate the final distribution of the excitation among the different chromophore units.

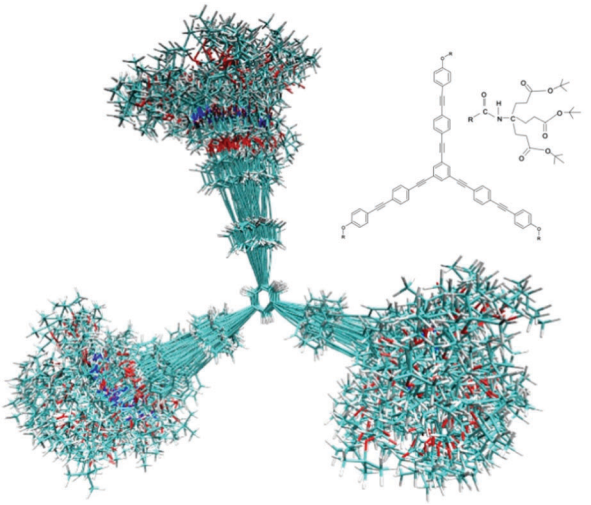

Fig. 1 Chemical structure of dendrimer **1** and the superposition of snapshots obtained from ground state molecular dynamics in THF.

The paper is organized as follows. Both experimental and theoretical methods are described in Section II, the results are presented and discussed in Section III and finally Section IV summarizes our findings and conclusions.

Methods

Computational methods

The photoexcitation and subsequent electronic and vibrational energy relaxation and redistribution of **1** have been simulated using the NA-ESMD[39,52] method. NA-ESMD combines the fewest switches surface hopping (FSSH) algorithm[53,54] with "on the fly" analytical calculations of excited-state energies,[55–57] gradients,[58,59] and non-adiabatic coupling terms.[39,60–62] Correlated excited states are calculated using the collective electron oscillator (CEO) method[63–65] with the configuration interaction singles (CIS) formalism implemented with the semiempirical AM1 Hamiltonian.[66] The instantaneous decoherence approach[67] is introduced in order to account for divergent quantum wavepackets and classical populations. The method resets the quantum amplitude of the current state to unity after every attempted hop. NA-ESMD has been successfully applied to a series of different building blocks and PE dendrimers,[39,43] providing a sufficiently accurate description of intramolecular energy transfer and transient exciton localization/delocalization during the photoinduced dynamics of these molecular systems. Further details of the NA-ESMD approach, implementation, advantages and testing parameters can be found in our previous work.[39,52,68]

During NAESMD simulations, the intramolecular electronic energy redistribution is followed by computing the time-dependent localization of the electronic transition density for the α current state. The diagonal elements of the calculated transition density matrices $(\rho^{g\alpha})_{nn}$ (index n refers to atomic orbital (AO) basis functions) represent the changes in the distribution of the electronic density induced by photoexcitation from the ground state g to an excited electronic α state.[69] Therefore, the transition

density localized on each linear PE unit or branch i at each time of the NA-ESMD simulations can be written as:

$$\rho^{g\alpha}_{\text{branch},i}(t) = \sum_{n_A} \left(\rho^{g\alpha}_{n_A n_A}(t)\right)^2 \quad (1)$$

where the index A runs over all atoms in a given linear PE branch.

The initial conditions for NA-ESMD simulations have been generated from an equilibrated ground state molecular dynamics simulation of **1** solvated with 1958 explicit tetrahydrofuran (THF) molecules with periodic boundary in a box with density = 0.891 g cm^{-3}. This was carried out using the AMBER 12 software package[70–73] using the GAFF (General Amber Force Field).[74,75] During simulations, a time step of 1 fs has been used and temperature was equilibrated employing a Langevin thermostat (γ = 2.0). Electrostatic potential (ESP) derived charges for previously optimized **1** geometry were obtained using single-point BLYP/6-31G* calculations and the Merz-Kollman scheme. Restricted ESP (RESP) charges[76,77] were obtained imposing symmetry on equivalent atom types. RESP charges for **1** are summarized in Fig. S1 (ESI†). After minimization, the system was heated to 300 K for 100 ps. Thereafter, 40 ns of NPT molecular dynamics simulations were performed. The system was equilibrated for 30 ns before starting to collect sets of NA-ESMD initial conditions at 20 ps intervals for 10 ns. The collected set of initial conditions was finally relaxed during a short MD run using the semiempirical AM1 Hamiltonian and explicit THF molecules have been removed.

Four hundred (400) independent NA-ESMD simulations were started from these initial configurations after vertical excitation to an initial excited state α, with the frequency Ω_α, selected according to the Frank–Condon window defined as $g_\alpha(r,R) = f_\alpha \exp[-T^2\ (E_{\text{laser}} - \Omega_\alpha)^2]$ where E_{laser} is the energy of the laser pulse centered at 383 nm and f_α represents the normalized oscillator strength for the α state, both expressed in units of fs^{-1}. We considered a Gaussian laser pulse, $f(t) = \exp(-t^2/2T^2)$, with T = 42.5 fs corresponding to a FWHM (Full Width at Half Maximum) of 100 fs. Each NA-ESMD simulation was run for 500 fs using a Langevin Thermostat to keep the temperature at 300 K with a friction coefficient of 2.0 ps^{-1}. A new random seed has been used for each NA-ESMD simulation in order to avoid synchronicity effects between them.[78] The bulky end-groups have been removed before the NA-ESMD simulations. Five electronic states and their corresponding nonadiabatic couplings were included in the simulations. A classical time step of 0.1 fs has been used for nuclei propagation and a quantum time step of 0.025 fs has been used to propagate the electronic degrees of freedom. In order to identify and deal with trivial unavoided crossings, the quantum time step was further reduced by a factor of 40 in the vicinity of such crossings.[79] More details concerning the NA-ESMD implementation and parameters can be found elsewhere.[39,52,68]

Experimental method

Compact dendrimers consisting of a backbone containing PE chromophores with bulky branched *t*-butyl ester ending groups were prepared using a convergent method described in detail in separate publications.[80]

Steady-state characterization was performed using UV-Vis absorption and fluorescence emission spectra. Sample concentrations for steady-state characterization were kept below 1 μM to avoid any aggregation[81] or excimer formation,[32] yielding optical densities less than 0.1 cm^{-1}.

We explored excited-state dynamics by time-resolved photoluminescence as a function of excitation and detection wavelengths. Fluorescence in the picosecond time-regime was characterized using the up-conversion technique.[40] Up-conversion allows the measurement of the temporal evolution of the fluorescence based on the sum-frequency mixing of the emission of molecules with an ultrafast gate pulse in a nonlinear crystal.[82] Tunable excitation pulses (300–400 nm) are derived from the 4th harmonic of the signal output of an optical parametric amplifier (OPA), pumped by a commercial Ti-sapphire laser system consisting of a Ti–Sapphire oscillator (Tsunami, Spectra-Physics) and a subsequent amplifier (Spitfire, Spectra-Physics) with a repetition rate of 1 kHz. After excitation of the sample, the fluorescence is collected using two off-axis parabolic mirrors, and the excited volume imaged onto a 0.5 mm thick β-barium borate crystal. A portion of the direct output of the amplified laser system (20 μJ pulse^{-1}) is weakly focused (50 cm focal length) on the same crystal and spatially overlapped with the imaged fluorescence. The up-converted UV signal is collimated and directed to a 0.25 m monochromator (Oriel Cornerstone 260) to be dispersed and detected by a visible-blind photomultiplier tube (Hamamatsu R7154). Crystal tuning combined with scanning of the delay between excitation and gate pulses allows measurement of the temporal evolution of the fluorescence at particular emission wavelengths (for details see ref. 40). The polarization of the excitation beam is controlled using a Berek Compensator. Pump pulses with energies lower than 40 nJ and a beam diameter of at least 200 μm are used to avoid photo bleaching and to maintain a linear optical response. The sample solutions, with concentrations below 10 μM (less than 0.15 mm^{-1}), are stirred during the experiments to ensure exposure of fresh volumes with every laser shot and their photostability is checked before, during, and after each up-conversion experiment. Steady-state spectra of these samples were compared with lower optical density solutions (less than 0.01 mm^{-1}) used for photophysical characterization and no changes in the spectra were observed due to aggregation or self-absorption. The time resolution of the experiment is measured by the cross-correlation of scattered pump and gate pulses yielding excitation pulses with FWHM ~270 fs at 350 nm. This instrument response function is used for the convolution of decay and rise time functions to fit the experimental data. Multiple scans are combined with 4000 laser shots averaged at each time step.

Results and discussion

We study the photoinduced dynamics of the first generation PE dendrimer (**1**), both from experimental and theoretical points of view. Fig. 1 shows the chemical structure based on three

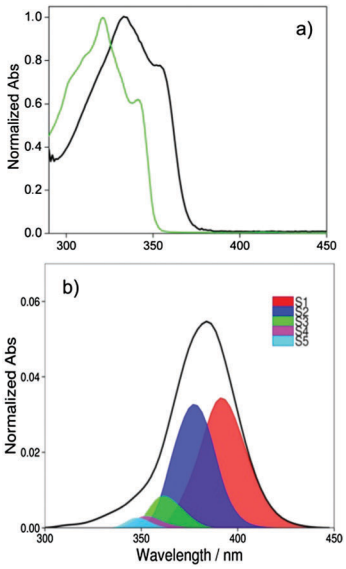

Fig. 2 (a) Steady state absorption spectra of **1** (black) and 1,4-bis(phenylethynyl)benzene (green) in THF; (b) simulated absorption spectra with separated contributions from the different excited states.

branches of equivalent, linear 1,4-bis(phenylethynyl) (PE) units, connected through the *meta* position to a central group. The end of each branch is capped with an alkoxy substituent connected to a dendritic-ester (R). The presence of these dendritic-ester groups makes the dendrimer soluble in organic solvents like THF but does not affect its photophysical properties.

The experimental and computed absorption spectra of **1** and the linear building block 1,4-bis(phenylethynyl) (Fig. S2, ESI†) at room temperature in THF are shown in Fig. 2, and the measured emissions are shown in the ESI† (Fig. S3). The experimental results show that the shape of the absorption spectra is quite similar for both molecules; emission of 1,4-bis(phenylethynyl)-benzene shows a clear vibronic structure while the emission of **1** is broad and featureless. Since the calculations do not include vibronic bands, these features are not expected to appear in the simulated spectra. The computed spectra appear at slightly lower energies than the experimental, an effect already observed in other similar molecules[35,43,83–85] which might be related to a difference in the solvent properties and the level of QM theory used but which does not change the understanding of the photophysical processes. The computed as well as the experimental absorption of dendrimer **1** display a red shift relative to the spectra of 1,4-bis(phenylethynyl); 36 nm and 12 nm respectively. The effect of alkoxy substituents in PE dendrimers has been previously reported.[46] Yoshida and coworkers[86] synthesized oligo(*p*-phenylene ethynylene)s as rod shaped π conjugated systems and characterized their photophysical properties. They observed red-shifts in the absorption and emission maxima, and an enhancement in the molar absorptivity of the oligomers as they are substituted with alkoxy groups in the *para* position. This effect was attributed to the alkoxy groups enabling electron donation to the PE units. Kolandaivel and coworkers[85] calculated the absorption and emission spectra of substituted and unsubstituted phenylene-ethynylene oligomers using time-dependent density functional theory (TDDFT), obtaining good agreement with the experiments, though the calculated red shifts were larger than the experimental ones. They concluded that the substitution with electron withdrawing or donating groups has a significant effect on the spectra. The red shift absorption spectrum of **1** compared to that of 1,4-bis(phenylethynyl) can also be related to rotations of the phenyl rings. It is known that the absorption spectra of PE oligomers are strongly affected by the rotation of the phenylene rings.[68,87] In the ground state, the energy barrier for the rotation of the phenylene rings is very low (near k_BT, 0.59 kcal mol^{-1} for diphenylacetylene in the gas phase) and the ground-state potential is shallow.[87] Nevertheless, higher energy barriers for ring-rotation are expected for **1** due to the presence of bulky branched *t*-butyl ester ending groups. Therefore, dendrimer **1** becomes more planar and with more extended conjugation lengths than the corresponding individual linear 1,4-bis(phenylethynyl) units.

The computed spectrum in Fig. 2 (bottom panel) shows the contributions from each excited state to the overall absorption band. The absorption band is composed of contributions from S_1 (46%), S_2 (37%), and S_3 (9%) states, with smaller contributions from higher energy states. In order to investigate the extent of coupling between the linear PE units in the different electronic excited states we analyze the distribution of values for the transition density (TD) found on each linear PE branch *i*, $\rho^{g\alpha}_{branch,i}(0)$ (α = 1, 2, 3), for the ensemble of the initial ground state conformational sampling. For each excited state S_α, if the initial TD were localized in only one i branch we would expect a sharp distribution near $\rho^{g\alpha}_{branch,i}(0) = 1$, whereas a fully delocalized TD would have a distribution around $\rho^{g\alpha}_{branch,i}(0) = 0.33$ for all branches. We have computed the localization of the TDs in each branch for each of the independent conformations sampled, and plotted the distributions of those TDs (at $t = 0$) in Fig. 3. These wide distributions arise due to diverse conformations in the room temperature ensemble leading to electronic states with contributions from different sites. This analysis of the spatial distribution of the transition densities allows understanding the nature of the electronic states, which are labeled according to their increasing energies but whose composition might change as the molecule samples different conformations.[39,84] The branches in Fig. 3 are labeled as I for the branch with the highest value of $\rho^{g\alpha}_{branch,i}(0)$, II for the next value of $\rho^{g\alpha}_{branch,i}(0)$, and III for the branch with the lowest value of $\rho^{g\alpha}_{branch,i}(0)$ for the $S_1 \leftarrow S_0$ transition.

The top panel in Fig. 3 shows the distribution of the TD in the different branches for S_1. That panel clearly shows that S_1 is mostly localized in a single branch (I) with very much less TD in branch II and almost no TD in branch III. The middle panel shows the TD distribution of S_2 among the three branches, while the lower panel shows the distribution of TD from S_3. These two panels establish that neither state S_2 nor S_3 contribute to the TD for branch I, since in both cases branch I has a sharp distribution near 0. State S_2 has its TD distributed with a slight asymmetry between the other two branches, while S_3 shows an almost mirror image for the distribution. We learn

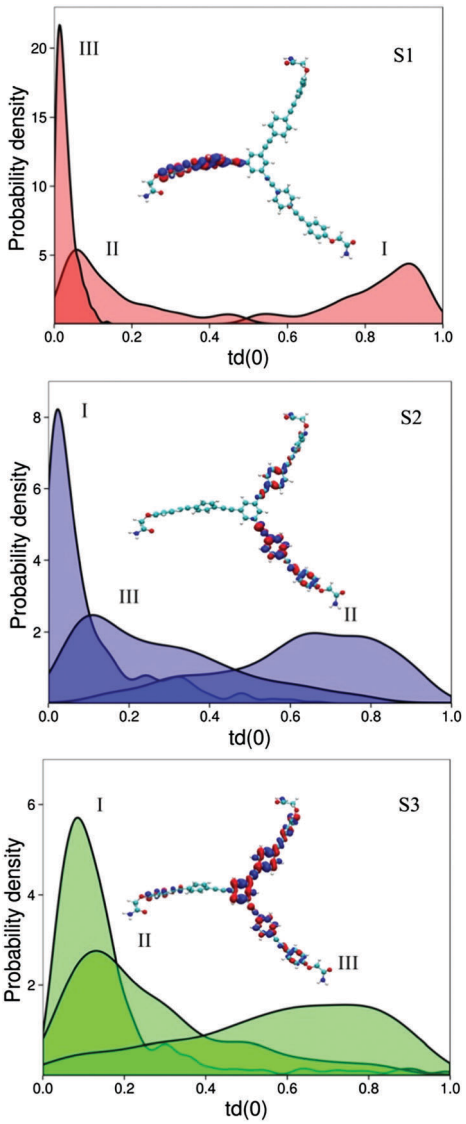

Fig. 3 Distribution over all initial configurations of the TD in each branch among the different states. The branches are labeled I, II, and III according to their values of $\rho^{g\alpha}_{branch,i}(0)$ for the $S_1 \leftarrow S_0$ transition, with I having the highest values in S_1 and III the lowest. Middle and lower panel show the $\rho^{g\alpha}_{branch,i}(0)$ for the $S_2 \leftarrow S_0$ and $S_3 \leftarrow S_0$ transition respectively. The labels of the branches are the same for all plots.

from this figure that branches II and II show excited state population from two different states, in contrast to the behavior of branch I, which is only populated by S_1.

These distributions can be rationalized in simple terms when one thinks about the D_{3h} symmetry this dendrimer will adapt when fully minimized in its ground electronic state. In this case, one can assign site energies for each branch with some weak coupling between them and the energies and orbitals can be analytically obtained within a Frenkel Exciton model.[88–90] In that case, one finds that there is one state mostly localized in one branch, with two other states delocalized between the other two branches, in agreement with the results presented here at room temperature.

Given the different patterns of branch localization for the different excited states, the photoinduced dynamics of the $S_n \rightarrow S_m$ electronic relaxation processes will also involve inter-branch energy exchange. The localization/delocalization process among equivalent dendrimer branches can be investigated using time-resolved emission anisotropy in the femtosecond time-scale. The sample is excited with linearly polarized light, and the emission as a function of time is detected selecting either parallel or perpendicular polarizations, compared to the initially polarized plane. These experiments provide valuable information about the excited state dynamics and the extent of inter-branch couplings by measuring the ultrafast depolarization changes following the excitation of Ph_3PG-1. Since the loss of anisotropy due to the rotation of molecules occurs on the nanosecond time-scale it is possible to characterize faster processes without interference from the rotational diffusion. The ultrafast up-conversion technique was used to explore the excited-state dynamics of dendrimer **1**. The dendrimer was dissolved in THF and excited at 340 nm (near the absorption maximum) while the emission was detected at 376 nm. The time-resolved anisotropy is calculated using the experimental perpendicular and parallel fluorescence decay data (see the inset in Fig. 4). The individual polarized emission intensities are fitted with a sum of exponentials convoluted with the instrument response function. The experimentally measured anisotropy is plotted with the resultant from the fitting of the individual components. The result is a very fast time anisotropy decay component of 330 fs. Other parameters used in this fitting were kept fixed: a very long decay time constant obtained from TCSPC measurements and a 3 ps time component characterized by using up-conversion measurements and assigned to vibrational cooling (*vide infra*). The final anisotropy values are slightly above 0.1, which is the expected value for a planar configuration.

In order to simulate the fluorescence anisotropy using NA-ESMD simulations, we need to compute the time correlation function of the normalized absorption dipole moment of

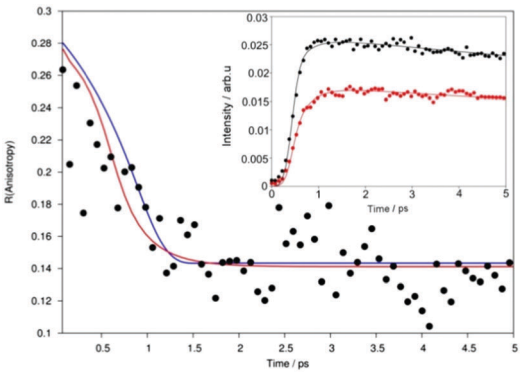

Fig. 4 Fluorescence anisotropy data for dendrimer **1** in THF. Experimental decay is shown in black, fitting in red, and simulated in blue. Inset: Time-resolved fluorescence data at parallel polarization (black dots) and perpendicular polarization (red dots) with their fitting given in solid lines. The fits are obtained by convolution with a 300 fs IRF.

1 at time zero, $\vec{\mu}_A(t = 0)$, and its normalized emission dipole moment at time t, $\vec{\mu}_E(t)$:[91]

$$C_{sim}(t) = \frac{I_{\parallel} - I_{\perp}}{I_{\parallel} + 2I_{\perp}} = \frac{2}{5}\langle P_2\{\vec{\mu}_A(0) \cdot \vec{\mu}_E(t)\}\rangle \qquad (2)$$

where I_I and $I_\perp$ are the intensities of fluorescence polarized parallel and perpendicular to the plane of polarization of the exciting radiation pulse, respectively. $P_2(x) = (3x^2 - 1)/2$ is the second-order Legendre polynomial. This equation assumes an ensemble of fluorophores with random isotropic initial orientation and the angular brackets denote the average over all the trajectories. The fluorescence anisotropy signal $R(t)$ is then obtained by calculating the convolution of $C_{sim}(t)$ with a Gaussian laser pulse whose width (300 fs FWHM) corresponds to the pulsewidth used in the experiments. The resulting fluorescence anisotropy curve is plotted in Fig. 4 (blue line), achieving a remarkable agreement with experiments.

Varnavski *et al.* used similar time-resolved anisotropy measurements on dendrimers to investigate fast energy delocalization kinetics.[92] They studied dendrimers having two types of symmetries (C_3 and T_d). In both cases, they observed anisotropy decays on the femtosecond time-scale. The rate of the energy delocalization process was strongly dependent on the nature of the central moiety. In the case of a nitrogen core, delocalization was faster as it enables strong coupling among the linear segments (35 fs). When the nitrogen was replaced with an adamantine core, delocalization got slower revealing weaker coupling (880 fs). Ruseckas *et al.*[93] described a sub 100 fs process in which nuclear relaxation leads to a spread of the exciton in a larger area, thus changing the effective orientation of the transition dipole moment.

In dendrimer **1**, the initial anisotropy value of $R(0) = 0.28$ is lower than the expected $R_{max} = 0.4$ for spherical systems leading us to conclude that an ultrafast process is masked by a convolution with the instrument response function. The initially computed excited state shows some degree of localization (Fig. 3). As energy transfer occurs, the redistribution of the transition density among the different branches will lead to the scrambling of the transition dipole orientation. This scrambling of the orientation of the transition dipole can occur through two plausible mechanisms.

In one case, a true delocalization of the wavefunction due to strong coupling among equivalent chromophores or due to nuclear relaxation.[93] Another possibility considers a wavefunction that maintains its localized nature in an individual branch, but hops around from one branch to another driven by weakly coupled chromophores.

The robust match between our experimental and simulated anisotropy results allows us to use the computational results to understand the mechanism behind the ultrafast loss of polarization anisotropy. We start by computing the excited state dynamics of the dendrimer and following the population of a given excited state (S_n) in time, as shown in Fig. 5 (top panel). Excitation is induced at the energy corresponding to the maximum of its absorption spectrum (383 nm), and takes into account the presence of several excited states in accordance to their contribution to the absorption spectrum. The initial state for NA-ESMD simulations is almost equivalently distributed between the S_1 and S_2 excited states with an almost negligible contribution from S_3 and nothing for states with $n > 3$. After photoexcitation, an efficient ultrafast energy transfer takes place driving all the population to the lowest excited state (S_1) within the first 100 fs.

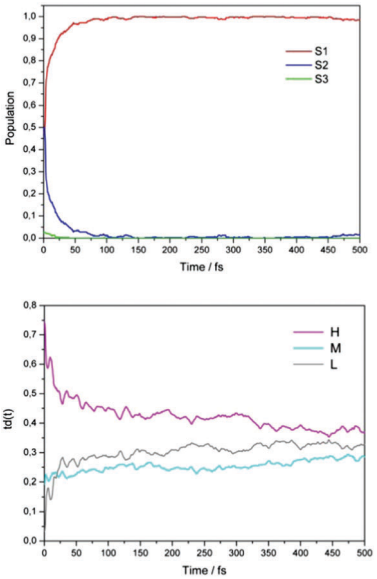

Fig. 5 Calculated time evolution of populations shown using a state (top) or spatial (low) descriptor. These plots show the transition densities averaged over all the members of the ensemble. The spatial descriptor assigns as high (H), medium (M) and low (L) the branches with highest to lowest transition density at $t = 0$.

Since changes in the nuclear coordinates during molecular dynamics can change the localization patterns of the TD without changes in the excited state label, the population of the excited states cannot be used to identify intra- or inter-branch energy transfers. Therefore, the final electronic relaxation to the adiabatic S_1 state, reported as the population increase in the lowest energy excited state (as shown in the Fig. 5 top panel) cannot be directly used to identify intra- or inter-branch energy transfers. In order to elucidate this feature, Fig. 5 compares the variation in time of the population in each adiabatic state (top panel) with the average fraction of electronic transition density spatially localized on the different branches (bottom panel). In the lower panel, for each trajectory we label the three branches according to their fraction of transition density high (H), medium (M), and low (L) at time = 0. During the time of measurement, the excitation experiences an ultrafast inter-branch migration that leads to a final scrambling of the spatial information. It is interesting to note that this spatial scrambling of the exciton takes place at a slower pace than the population transfer among states; comparison of top and bottom panels shows that although by $t = 75$ fs all the populations have reached S_1, the population of the spatial distributions continues to evolve until at least 500 fs.

In the spatial description an ultrafast inter-branch exchange of the excitation from the initial highest to medium and lowest

branches is observed during the first ~5–10 fs. The absence of an energy gradient leads to an ultrafast energy redistribution among isoenergetic chromophore units. Analysis of the inter-branch transition density exchanges shows that most of the stepwise variations involving large ΔTD values occur within the first 10 fs, after which we only observe ΔTDs of small magnitude, which continue to happen for long periods of time.

These results resemble those obtained in previous simulations of the photoinduced energy transfer between two chromophore units of the coupled anthracene dimer dithia-anthracenophane (DTA). The latter have also shown equivalent final energy redistribution among chromophore units,[94] with half of the trajectories finishing completely localized on the same monomer on which the initial excitation was located, and the other half of them becomes fully localized on the other monomer. The initial nonadiabatic coupling between states leads to an ultrafast exchange of energy between monomers while thermally induced geometric distortions and vibrational relaxation lead to localized electronic states.

Since Fig. 5 shows ensemble-average values, it is not possible to elucidate whether the spatial scrambling is due to hopping between sites or due to delocalization of the wavefunction among the different branches. A proper interpretation of the experimental data, and the understanding of the excited state dynamics can be obtained by the analysis of the distributions of the members of the ensemble. The critical role of choosing the suitable descriptor can be better understood by evaluating the evolution of the complete distributions of transition density in each branch.

Fig. 6 shows the distributions of TD among the three branches at different times within the system's evolution. For each branch, we present the TD corresponding to the sum of the contributions from three excited states. Immediately after excitation, the TD is broadly and unevenly distributed between two branches while a third branch is not excited. As the excited state dynamics evolves, the transitions become spatially localized.

By the end of the simulations (500 fs), the distribution of the probability of obtaining TD values shows that the TD is localized in a given branch (sharp bands with TD ~ 1) thus the other two branches must have TD ~ 0. The similar plots for the three branches at long times show the obvious answer where after the dynamics are concluded, the ensemble distribution has about a third of the configurations with TD confined in one given branch, and the choice of branch is randomly distributed, giving rise to the averages seen in Fig. 5.

These results unequivocally demonstrate a mechanism of the initial confinement of the spatial excitation within an individual branch followed by hopping between localized transition densities. The first process is due to the $S_1 \leftarrow S_2$ energy transfer and occurs in a very fast timescale, while the second process corresponds to inter-branch energy transfer while the population remains in S_1 and it occurs in a slower timescale.

It is interesting to compare the results for this symmetric dendrimer with those of the previously studied unsymmetrical dendrimer.[43] In that molecular system, energy bias and coupling

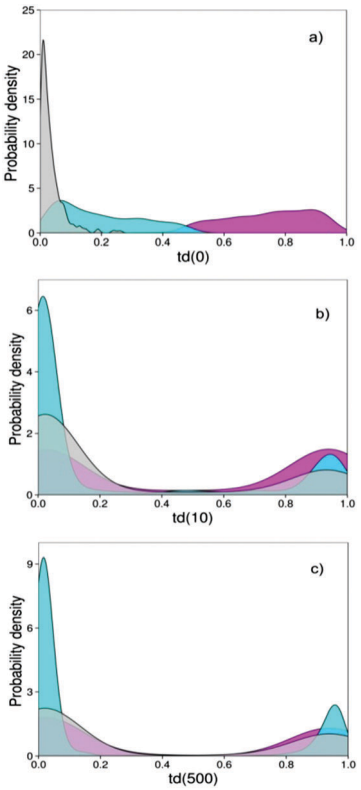

Fig. 6 Evolution in time of the distribution of fraction of electronic transition density localized on individual branches. The branches are classified according to their initial value of the fraction of transition density: high (magenta), medium (cyan) and low (gray) and they are graphed at (a) t = 0, (b) 10 and (c) 500 fs.

to vibrational modes point to a localization of the excited state in one segment of the dendritic backbone before the final step of energy transfer to the lowest excited state. In the work presented here, immediately after photoexcitation the spatial distribution corresponds to a slightly delocalized picture due to the contribution from different states that reside in complementary branches. Following an initial high-activity period driven by population transfer from S_2 to S_1, the changes in transition density become smaller and last for several hundreds of femtoseconds implying that the branches become less coupled. As a result, random exciton self-trapping on different PE units is observed with the final similar probabilities for each branch to retain significant contributions of the lowest excited-state electronic transition density.

Conclusions

The photoexcitation and subsequent ultrafast spatial redistribution and electronic energy relaxation on a first generation dendrimer have been studied combining theoretical and experimental studies. Upon excitation, an efficient ultrafast $S_2 \rightarrow S_1$ energy transfer takes place. Time resolved anisotropy shows ultrafast scrambling of the transition dipole moment orientation in *ca.* 300 fs, raising the question of potential

coherent delocalization of the wavefunction. To understand the excited state dynamics and the mechanism behind the energy transfer we must choose a suitable set of descriptors, which in this case correspond to the spatial distribution of the excited state wavefunctions.

Our results reveal a consistent picture of the ultrafast loss of anisotropy due to an initial energy transfer between adiabatic states. This process is followed by random exciton self-trapping on different units as the branches become less coupled. The final ensemble describes the random distribution of self-trapped excitons on different PE units with each branch retaining a similar probability of significant contribution of the transition density to the lowest electronic excited-state. This process of spatial redistribution among chromophore units is driven by the lack of an energy gradient. The experimental loss of polarized emission can therefore be assigned to the confinement of the electronic wavefunction in a single branch and its hopping between the branches rather than to its expansion over the whole dendrimer.

Acknowledgements

This work was partially supported by the National Science Foundation Grant (CHE-1058638), CONICET, UNQ, ANPCyT (PICT-PICT-2014-2662) and the U.S. Department of Energy and Los Alamos LDRD funds. Los Alamos National Laboratory is operated by Los Alamos National Security, LLC, for the National Nuclear Security Administration of the U.S. Department of Energy under contract DE-AC52-06NA25396. We acknowledge support from the Center for Integrated Nanotechnology (CINT) and the Center for Nonlinear Studies (CNLS) at LANL. The samples were synthesized by Dr Fude Feng and Kirk Schanze at the University of Florida.

References

1 J. Holdren, *Science*, 2007, **315**, 737.
2 G. Scholes, G. Fleming, A. Olaya-Castro and R. van Grondelle, *Nat. Chem.*, 2011, **3**(10), 763.
3 P. Frischmann, K. Mahata and F. Wurthner, *Chem. Soc. Rev.*, 2013, **42**(4), 1847.
4 S. Mathew, A. Yella, P. Gao, R. Humphry-Baker, B. Curchod, N. Ashari-Astani, I. Tavernelli, U. Rothlisberger, M. Nazeeruddin and M. Gratzel, *Nat. Chem.*, 2014, **6**(3), 242.
5 A. Halpin, P. Johnson, R. Tempelaar, R. Murphy, J. Knoester, T. Jansen and R. Miller, *Nat. Chem.*, 2014, **6**(3), 196.
6 G. S. Engel, T. R. Calhoun, E. L. Read, T.-K. Ahn, T. Mancal, Y.-C. Cheng, R. E. Blankenship and G. R. Fleming, *Nature*, 2007, **446**(7137), 782.
7 D. Andrews, *J. Mater. Res.*, 2012, **27**, 627.
8 A. Adronov and J. Fréchet, *Chem. Commun.*, 2000, 1701.
9 X. Hu, A. Damjanovic, T. Ritz and K. Schulten, *Proc. Natl. Acad. Sci. U. S. A.*, 1998, **95**, 5935.
10 F. Caycedo-Soler, F. Rodriguez, J. Quiroga and N. Johnson, *Phys. Rev. Lett.*, 2010, **104**, 158302.
11 D. Tomalia, H. Baker, J. Dewald, M. Hall, G. Kallos, S. Martin, J. Roeck, J. Ryder and P. Smith, *Macromolecules*, 1986, **19**(9), 2466.
12 G. Newkome, Z. Yao, G. Baker and V. Gupta, *J. Org. Chem.*, 1985, **50**(11), 2003.
13 J. Fréchet, *Proc. Natl. Acad. Sci. U. S. A.*, 2002, **99**(8), 4782.
14 J. Fréchet, *J. Polym. Sci., Part A: Polym. Chem.*, 2003, **41**(23), 3713.
15 C. Schalley, F. Vögtle, V. Balzani, P. Ceroni, M. Maestri, C. Saudan and V. Vicinelli, in *Luminescent Dendrimers. Recent Advances. In Dendrimers V*, ed. C. Schalley and F. Vögtle, Springer, Berlin/Heidelberg, 2003, pp. 159–191.
16 D. Smith and F. Diederich, *Chem. – Eur. J.*, 1998, **4**(8), 1353.
17 P. Rajakumar, V. Kalpana, S. Ganesan and P. Maruthamuthu, *New J. Chem.*, 2013, **37**(11), 3692.
18 P. Froehling, *Dyes Pigm.*, 2001, **48**(3), 187.
19 G. Denti, S. Campagna, S. Serroni, M. Ciano and V. Balzani, *J. Am. Chem. Soc.*, 1992, **114**(8), 2944.
20 C. Devadoss, P. Bharathi and J. S. Moore, *J. Am. Chem. Soc.*, 1996, **118**, 9635.
21 S. Gilat, A. Adronov and J. Fréchet, *Angew. Chem., Int. Ed.*, 1999, **38**(10), 1422.
22 Z. Peng, J. Melinger and V. D. Kleiman, *Photosynth. Res.*, 2006, **87**(1), 115.
23 A. Bosman, H. Janssen and E. Meijer, *Chem. Rev.*, 1999, **99**(7), 1665.
24 V. Balzani, P. Ceroni, M. Maestri and V. Vicinelli, *Curr. Opin. Chem. Biol.*, 2003, **7**(6), 657.
25 A. Nantalaksakul, D. Reddy, C. Bardeen and S. Thayumanavan, *Photosynth. Res.*, 2006, **87**(1), 133.
26 T. Aida, D.-L. Jiang, E. Yashima and Y. Okamoto, *Thin Solid Films*, 1998, **331**(1–2), 254.
27 S. Mukamel, *Nature*, 1997, **388**, 425.
28 J. M. Fréchet, *Science*, 1994, **263**(5154), 1710.
29 S. Swallen, Z. Zhu, J. Moore and R. Kopelman, *J. Phys. Chem. B*, 2000, **104**(16), 3988.
30 Z. Xu, M. Kahr, K. L. Walker, C. L. Wilkins, J. S. Moore and J. S. M. Jj, *J. Am. Chem. Soc.*, 1994, **116**(11), 4537.
31 R. Kopelman, M. Shortreed, Z. Y. Shi, W. Tan, Z. Xu, J. S. Moore, A. Bar-Haim and J. Klafter, *Phys. Rev. Lett.*, 1997, **78**, 1239.
32 S. F. Swallen, R. Kopelman, J. S. Moore and C. Devadoss, *J. Mol. Struct.*, 1999, **486**, 585.
33 M. R. Shortreed, S. F. Swallen, Z. Y. Shi, W. Tan, Z. Xu, C. Devadoss, J. S. Moore and R. Kopelman, *J. Phys. Chem. B*, 1997, **101**, 6318.
34 J. S. Melinger, Y. C. Pan, V. D. Kleiman, Z. H. Peng, B. L. Davis, D. McMorrow and M. Lu, *J. Am. Chem. Soc.*, 2002, **124**(40), 12002.
35 S. Fernandez-Alberti, V. D. Kleiman, S. Tretiak and A. E. Roitberg, *J. Phys. Chem. A*, 2009, **113**(26), 7535.
36 S. Fernandez-Alberti, V. D. Kleiman, S. Tretiak and A. E. Roitberg, *J. Phys. Chem. Lett.*, 2010, **1**, 2699.
37 S. Fernandez-Alberti, A. E. Roitberg, V. D. Kleiman, T. Nelson and S. Tretiak, *J. Chem. Phys.*, 2012, **137**(22), 22A526.

38 T. Kobayashi, T. Okada, T. Kobayashi, K. Nelson, S. Silvestri, E. Atas, C. Mair, J. Melinger, Z. Peng and V. Kleiman, in *Ultrafast Phenomena XIV*, ed. A. Castleman, J. Toennies and W. Zinth, Springer, Berlin, Heidelberg, 2005, pp. 456–458.
39 T. Nelson, S. Fernandez-Alberti, A. E. Roitberg and S. Tretiak, *Acc. Chem. Res.*, 2014, **47**, 1155.
40 E. Atas, Z. H. Peng and V. D. Kleiman, *J. Phys. Chem. B*, 2005, **109**(28), 13553.
41 V. D. Kleiman, J. S. Melinger and D. Mc Morrow, *J. Phys. Chem. B*, 2001, **105**, 5595.
42 D. Kuroda, C. Singh, Z. Peng and V. Kleiman, *Science*, 2009, **326**(5950), 263.
43 J. F. Galindo, E. Atas, A. Altan, D. G. Kuroda, S. Fernandez-Alberti, S. Tretiak, A. E. Roitberg and V. D. Kleiman, *J. Am. Chem. Soc.*, 2015, **137**(36), 11637.
44 S. Kömürlü, S. H. Lee, T. McCarley, K. S. Schanze and V. D. Kleiman, *J. Phys. Chem. B*, 2011, **115**(51), 15214.
45 M. A. Soler, A. E. Roitberg, T. Nelson, S. Tretiak and S. Fernandez-Alberti, *J. Phys. Chem. A*, 2012, **116**(40), 9802.
46 K. Gaab, A. Thompson, J. Xu, T. Martnez and C. Bardeen, *J. Am. Chem. Soc.*, 2003, **125**(31), 9288.
47 M. Ranasinghe, M. Hager, C. Gorman and T. Goodson, *J. Phys. Chem. B*, 2004, **108**(25), 8543.
48 T. S. Ahn, A. L. Thompson, P. Bharathi, A. Müller and C. J. Bardeen, *J. Phys. Chem. B*, 2006, **110**(40), 19810.
49 F. Feng, S. H. Lee, S. W. Cho, S. Kömürlü, T. D. McCarley, A. Roitberg, V. D. Kleiman and K. S. Schanze, *Langmuir*, 2012, **28**(48), 16679.
50 J. Huang, L. Du, D. Hu and Z. Lan, *J. Comput. Chem.*, 2015, **36**(3), 151.
51 W. Ortiz, B. P. Krueger, V. D. Kleiman, J. L. Krause and A. E. Roitberg, *J. Phys. Chem. A*, 2005, **109**, 11512.
52 T. Nelson, S. Fernandez-Alberti, V. Chernyak, A. E. Roitberg and S. Tretiak, *J. Phys. Chem. B*, 2011, **115**, 5402.
53 J. C. Tully, *J. Chem. Phys.*, 1990, **93**, 1061.
54 S. Hammes-schiffer and J. C. Tully, *J. Chem. Phys.*, 1994, **101**(6), 4657.
55 S. Tretiak and S. Mukamel, *Chem. Rev.*, 2002, **102**(9), 3171.
56 V. Chernyak, M. F. Schulz, S. Mukamel, S. Tretiak and E. V. Tsiper, *J. Chem. Phys.*, 2000, **113**, 36.
57 S. Tretiak, C. M. Isborn, A. M. N. Niklasson and M. Challacombe, *J. Chem. Phys.*, 2009, **130**, 054111.
58 F. Furche and R. Ahlrichs, *J. Chem. Phys.*, 2002, **117**, 7433.
59 S. Tretiak and V. Chernyak, *J. Chem. Phys.*, 2003, **119**, 8809.
60 M. Tommasini, V. Chernyak and S. Mukamel, *Int. J. Quantum Chem.*, 2001, **85**, 225.
61 V. Chernyak and S. Mukamel, *J. Chem. Phys.*, 2000, **8**, 3572.
62 R. Send and F. Furche, *J. Chem. Phys.*, 2010, **132**, 044107.
63 S. Mukamel, S. Tretiak, T. Wagersreiter and V. Chernyak, *Science*, 1997, **277**(5327), 781.
64 S. Tretiak, V. Chernyak and S. Mukamel, *J. Chem. Phys.*, 1996, **105**, 8914.
65 S. Tretiak, W. M. Zhang, V. Chernyak and S. Mukamel, *Proc. Natl. Acad. Sci. U. S. A.*, 1999, **96**(23), 13003.
66 M. J. S. Dewar, E. G. Zoebisch, E. F. Healy and J. J. P. Stewart, *J. Am. Chem. Soc.*, 1985, **107**, 3902.
67 T. Nelson, S. Fernandez-alberti, A. E. Roitberg and S. Tretiak, *J. Chem. Phys.*, 2013, **138**, 224111.
68 T. Nelson, S. Fernandez-Alberti, V. Chernyak, A. E. Roitberg and S. Tretiak, *J. Chem. Phys.*, 2012, **136**(5), 054108.
69 C. Wu, S. V. Malinin, S. Tretiak and V. Y. Chernyak, *Nat. Phys.*, 2006, **2**(9), 631.
70 D. A. Case, T. A. Darden, T. E. Cheatham, III, C. L. Simmerling, J. Wang, R. E. Duke, R. Luo, R. C. Walker, W. Zhang, K. M. Merz, B. Roberts, S. Hayik, A. Roitberg, G. Seabra, J. Swails, A. W. Goetz, I. Kolossvai, K. F. Wong, F. Paesani, J. Vanicek, R. M. Wolf, J. Liu, X. Wu, S. R. Brozell, T. Steinbrecher, H. Gohlke, Q. Cai, X. Ye, J. Wang, M.-J. Hsieh, G. Cui, D. R. Roe, D. H. Mathews, M. G. Seetin, R. Salomon-Ferrer, C. Sagui, V. Babin, T. Luchko, S. Gusarov, A. Kovalenko and P. A. Kollman, *AMBER 12*, University of California, San Francisco, 2012.
71 R. Salomon-Ferrer, A. W. Goetz, D. Poole, S. L. Grand and R. C. Walker, *J. Chem. Theory Comput.*, 2013, **9**, 3878.
72 A. W. Goetz, M. J. Williamson, D. Xu, D. Poole, S. L. Grand and R. C. Walker, *J. Chem. Theory Comput.*, 2012, **8**, 1542.
73 S. L. Grand, A. W. Goetz and R. C. Walker, *Comput. Phys. Commun.*, 2013, **184**, 374.
74 J. Wang, R. Wolf, J. Caldwell, P. Kollman and D. Case, *J. Comput. Chem.*, 2004, **25**(9), 1157.
75 G. Mukherjee, N. Patra, P. Barua and B. Jayaram, *J. Comput. Chem.*, 2011, **32**(5), 893.
76 P. Cieplak, W. Cornell, C. Bayly and P. Kollman, *J. Comput. Chem.*, 1995, **16**, 1357.
77 C. Bayly, P. Cieplak, W. Cornell and P. Kollman, *J. Phys. Chem.*, 1993, **97**, 10269.
78 D. J. Sindhikara, S. Kim, A. F. Voter and A. E. Roitberg, *J. Chem. Theory Comput.*, 2009, **5**(6), 1624.
79 S. Fernandez-Alberti, A. E. Roitberg, T. Nelson and S. Tretiak, *J. Chem. Phys.*, 2012, **137**(1), 014512.
80 F. Feng, S. Lee, S. Cho, S. Kömürlü, T. McCarley, A. Roitberg, V. Kleiman and K. Schanze, *Langmuir*, 2012, **28**, 16679.
81 B. Davis, J. Melinger, D. McMorrow, Z. Peng and Y. Pan, *J. Lumin.*, 2004, **106**, 301.
82 H. Abramczyk, *Introduction to Laser Spectroscopy*, Elsevier, 2005.
83 S. Fernandez-Aberti, V. D. Kleiman, S. Tretiak and A. E. Roitberg, *J. Phys. Chem. Lett.*, 2010, **1**, 2699.
84 S. Fernandez-Alberti, A. E. Roitberg, V. D. Kleiman, T. Nelson and S. Tretiak, *J. Chem. Phys.*, 2012, **137**(22), 22A526.
85 N. Santhanamoorthi, K. Senthilkumar and P. Kolandaivel, *Mol. Phys.*, 2009, **107**(16), 1629.
86 A. Y. Yamaguchi, T. Tanaka, S. Kobayashi, Y. Matsubara and Z. Yoshida, *J. Am. Chem. Soc.*, 2005, **127**, 9332.
87 A. L. Thompson, K. M. Gaab, J. J. Xu, C. J. Bardeen and T. J. Martinez, *J. Phys. Chem. A*, 2004, **108**(4), 671.
88 F. Terenziani, C. Katan, E. Badaeva, S. Tretiak and M. Blanchara-Desce, *Enhanced two-photon absorption of organic chromophores: theoretical and experimental assessments*, 2008, vol. 20.

89 C. Katan, F. Terenziani, O. Mongin, M. H. V. Werts, L. Porres, T. Pons, J. Mertz, S. Tretiak and M. Blanchard-Desce, *J. Phys. Chem. A*, 2005, **109**, 3024.
90 C. Katan, S. Tretiak, M. H. V. Werts, A. J. Bain, R. J. Marsh, N. Leonczek, N. Nicolaou, E. Badaeva, O. Mongin and M. Blanchard-Desce, *J. Phys. Chem. B*, 2007, **111**(32), 9468.
91 A. Szabo, *J. Chem. Phys.*, 1984, **81**(1), 150.
92 O. P. Varnavski, J. C. Ostrowski, L. Sukhomlinova, R. J. Twieg, G. C. Bazan and T. Goodson, *J. Am. Chem. Soc.*, 2002, **124**(8), 1736.
93 A. Ruseckas, P. Wood, I. D. W. Samuel, G. R. Webster, W. J. Mitchell, P. L. Burn and V. Sundstrom, *Phys. Rev. B: Condens. Matter Mater. Phys.*, 2005, **72**(11), 1.
94 L. Alfonso Hernandez, T. Nelson, S. Tretiak and S. Fernandez-Alberti, *J. Phys. Chem. B*, 2015, **119**, 7242.